Journal of Molecular Graphics and Modelling 44 (2013) 136–144

Contents lists available at ScienceDirect

Journal of Molecular Graphics and Modelling

journal homepage: www.elsevier.com/locate/JMGM

Study of the interaction of *Huperzia saururus* Lycopodium alkaloids with the acetylcholinesterase enzyme

Marcelo Puiatti[a,*], José Luis Borioni[a], Mariana Guadalupe Vallejo[b], José Luis Cabrera[b], Alicia Mariel Agnese[b], María Gabriela Ortega[b], Adriana Beatríz Pierini[a,*]

[a] *Instituto de Investigaciones en Físico Química de Córdoba (INFIQC-CONICET), Departamento de Química Orgánica, Facultad de Ciencias Químicas, Universidad Nacional de Córdoba, Ciudad Universitaria, X5000HUA Córdoba, Argentina*
[b] *Instituto Multidisciplinario de Biología Vegetal (IMBIV-CONICET), Departamento de Farmacia, Facultad de Ciencias Químicas, Universidad Nacional de Córdoba, Ciudad Universitaria, X5000HUA Córdoba, Argentina*

ARTICLE INFO

Article history:
Received 29 March 2013
Received in revised form 14 May 2013
Accepted 27 May 2013
Available online 11 June 2013

Keywords:
Lycopodium alkaloids
Sauroxine
Acetylcholinesterase inhibitors
Docking
Molecular dynamics

ABSTRACT

In the present study, we describe and compare the binding modes of three Lycopodium alkaloids (sauroine, 6-hydroxylycopodine and sauroxine; isolated from *Huperzia saururus*) and huperzine A with the enzyme acetylcholinesterase. Refinement and rescoring of the docking poses (obtained with different programs) with an all atom force field helped to improve the quality of the protein–ligand complexes. Molecular dynamics simulations were performed to investigate the complexes and the alkaloid's binding modes. The combination of the latter two methodologies indicated that binding in the active site is favored for the active compounds. On the other hand, similar binding energies in both the active and the peripheral sites were obtained for sauroine, thus explaining its experimentally determined lack of activity. MM-GBSA predicted the order of binding energies in agreement with the experimental IC_{50} values.

1. Introduction

Alzheimer's disease (AD) is the most common cause of dementia in elderly people. Unfortunately, to date an effective cure or even preventive therapy remains elusive [1]. Most of the available treatments have only a palliative effect, providing a temporary retention of cognitive and memory functions, but without altering the disease's progression [2].

In the 1970s and in the 1980s the basis of the cholinergic hypothesis began to be understood [3], thereby providing for the first time a rational approach to the treatment of memory loss in AD. Improvements in cognitive abilities in AD patients were achieved by blocking or disrupting the acetylcholinesterase (AChE) activity with reversible inhibitors. After the pioneering findings of Inestrosa et al. [4,5], the amyloid hypothesis for the AD's pathogenesis was proposed, by which the accumulation of amyloid β (Aβ) aggregates triggers a cascade of neurotoxic events in the brain eventually leading to a widespread neuronal degeneration and hence to dementia. As a consequence, new anti-Alzheimer drug candidates focused on this problem, in order to modify the stage of the disease [6].

In silico methods were also used to enhance the understanding of AChE and to assist in the design of new inhibitors (AChEIs) [7–11]. The first computational studies were carried out with the *Torpedo Californica Acetylcholinesterase* (*Tc*AChE), whose first crystal structure appeared in 1991 [12]. This also helped understanding the function [13,14] and the interaction of the enzyme with the inhibitors. The residues responsible for the catalytic activity of AChE, the catalytic triad (Ser203, His447, Glu334) [15], are found at the bottom of a 20 Å deep gorge or cavity that constitutes the active site (AS) (see Fig. 1). In this gorge, there are also three other subsites, named after the binding of the acetylcholine: the anionic subsite (formed by Trp86, Tyr133, Glu202), the oxyanion subsite (Gly121, Gly122 and Ala204) and the acyl-binding subsite (Trp236, Phe295, Phe297 and Phe338). At the top of the gorge, there is a couple of aromatic residues, Tyr124 and Phe338, which form the so-called "bottleneck" that opens and closes and acts as a gate to the AS. Outside the gorge, next to the "entrance", there is another site called the peripheral anionic site (PAS), where the precursors of the Aβ are proposed to deposit before aggregation [16,17]. Moreover, it has been shown that molecules able to interact with both sites of AChE (i.e. a dual-site inhibitor) were able to prevent the aggregating activity of AChE toward Aβ as well as the hydrolysis of acetylcholine [18]. Therefore, inhibitors with the dual-site binding mode have recently been presented as a new therapeutic option [6].

* Corresponding authors.
E-mail addresses: mpuiatti@fcq.unc.edu.ar, marcelo.puiatti@gmail.com (M. Puiatti), adriana@fcq.unc.edu.ar (A.B. Pierini).

1093-3263/$ – see front matter © 2013 Elsevier Inc. All rights reserved.
http://dx.doi.org/10.1016/j.jmgm.2013.05.009

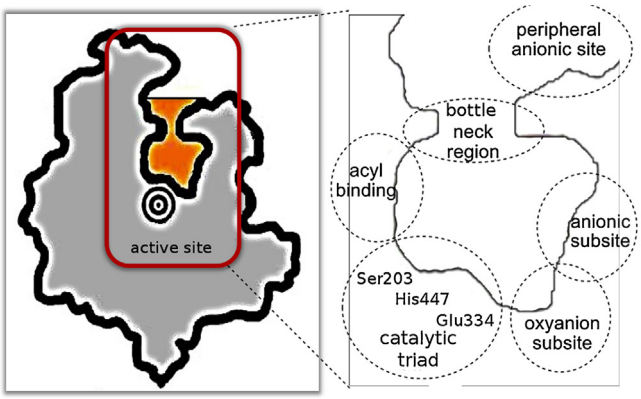

Fig. 1. Schematic description of the active site of the AChE and the corresponding subsites.

It is recognized that natural products can play an important role as inhibitors of the AChE, or as templates for the development of new synthetic AChEIs [19]. Among these compounds are found physostigmine (**1**) [20–22], huperzine A (**2**) [23,24], and galanthamine (**3**) [25,26]. Other AChEIs of relevance, but obtained by synthesis, are tacrine (**4**) [27], donepezil (**5**) [28,29] and rivastigmine (**6**) [30], the latter being a semi-synthetic derivative of **1**. Last but not least, there is a family of compounds originated by a fusion between the tacrine and huperzine A cores, namely the huprine family (**7**) [31,32], i.e. huprine X (**8**) [33,34], which also act as useful AChEIs, but are not yet approved by FDA. All these compounds bind to the bottom of the gorge and block the action of the catalytic triad [35–40] (Scheme 1).

Alkaloids are among the strongest AChEIs, and hence there is a constant search for new alkaloids with inhibitory properties. Over 200 Lycopodium alkaloids have been reported, but only some of them have shown to be good AChEIs [41]. A number of plants have also been used in traditional medicine for the treatment of memory and cognitive disorders, such as *H. serrata*, from which

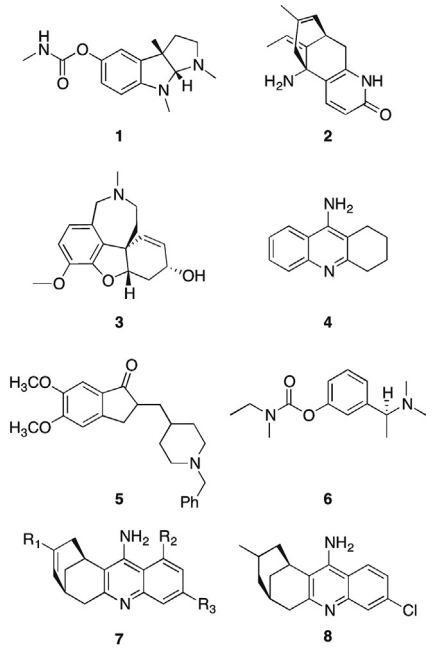

Scheme 1. AChE inhibitors.

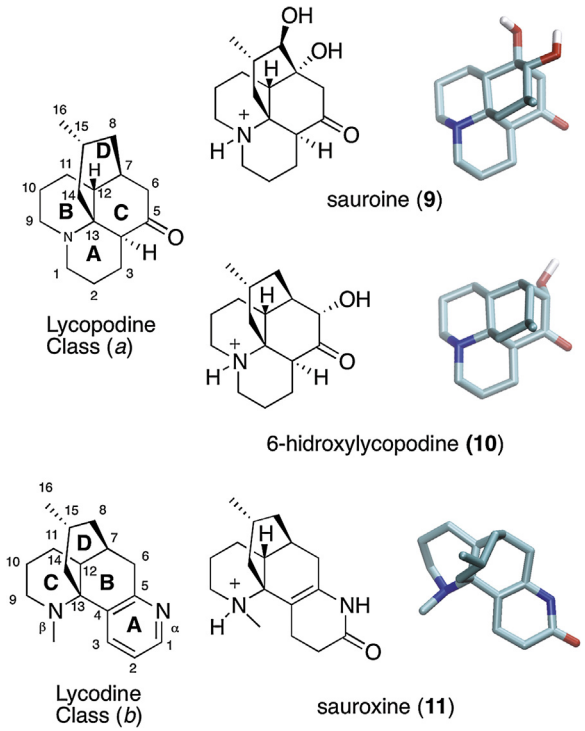

Scheme 2. Proposed AChEI extracted from *Huperzia saururus*.

some Lycopodium alkaloids with promising AChE inhibitory activity were obtained. With the aim of exploiting the properties of these alkaloids, based on Argentinian folk medicine, an investigation was conducted on *Huperzia saururus* (Lam.) Trevis. (Lycopodeaceae). This species is commonly known as “cola de quirquincho”, whose aerial parts are consumed as an infusion or a decoction because of their claimed folk use as an aphrodisiac [42] or for improving memory [43]. Previous studies on *H. saururus* collected in Pampa de Achala (Córdoba), Argentina, showed the presence of eight different alkaloids in a purified alkaloid extract, with sauroine (**9**), being the predominant one (Scheme 2) [21,44]. The purified alkaloid extract of *H. saururus* was shown to be active as an AChEI [45,46], although the major alkaloid (**9**) was not. The IC_{50} values for the Lycopodine Class of alkaloids were similar to those of other alkaloids from the same class [47] but based on the experimental information available, the Lycopodine type alkaloids may be less active than the Lycodine type.

In order to rationalize the relationship between the structure of the alkaloids and their activities, we studied the interaction of the alkaloids **9**–**11** (isolated from *H. saururus*, Scheme 2) with AChE by using the computational methods of docking and molecular dynamics (MD) simulations. For a better comprehension, compounds **9** and **10** were grouped together due to their structural similarities (both belong to Lycopodine Class (Scheme 2a)) and compound **11** was compared with **2**, which was used as a reference, as both are from the Lycodine Class (Scheme 2b) [48].

2. Materials and methods

2.1. Experimental information

2.1.1. Lycopodium alkaloids

Sauroine (**9**), 6-hydroxylycopodine (**10**) and sauroxine (**11**) were isolated, purified and identified as previously reported [21,44–46,49].

2.2. Anticholinesterase activity assay

2.2.1. Enzyme source

Erythrocyte membranes were used as the enzyme source and were obtained as previously informed [21,44–46].

2.2.2. Determination of the inhibitory effect

The acetyl cholinesterase assay was performed using the colorimetric method of Ellman and co-workers [50], with some modifications incorporated by our group. In order to calculate the activity, the following procedure was employed: 750 μL of phosphate buffer (50 mM, pH 7.2), containing 0.25 mM of 5,5′-dithiobis-2-nitrobenzoic acid (buffer + DTNB), 5 μL enzyme preparation, 25 μL of acetylthiocholine iodide 5 mM, and 100 μL of distilled water, were mixed and incubated for 30 min. Afterwards, the measurements were taken once every 30 s over the next 3 min, at 25 °C. All experiments were repeated three times. Different concentrations of sauroine (**9**), 6-hydroxylycopodine (**10**) and sauroxine (**11**), in a range of 2–700 μM, were required for 50% enzyme inhibition (IC_{50}). The IC_{50} values were estimated from a non-linear fitting of the concentration–response data, using the GraFit 6.0 software. Physostigmine salicylate was employed as the reference inhibitor for comparison of the anticholinesterase activity [21,44–46].

2.3. Computational methods

2.3.1. Docking simulations

The programs *Autodock 3* (*A3*) [51], *Autodock 4.2* (*A4.2*) [52] and *Autodock Vina* (*AV*) [53] were used for the docking simulations with the ff99 [54] force field charges for the protein residues. The starting coordinates of the protein were those of the X-ray structure 3LII [13] and all the water molecules were removed. The coordinates of the missing residues (Pro259, Gly260, Gly261, Thr262 and Gly263) were added with the side chain prediction tools included in *Maestro* [55]. The protonation states of the amino acids in the protein were assigned with the *H++ server* [56,57], and the ones of the residues in the catalytic gorge (His447, Glu334, Glu202 and Asp74) on the basis of previous representative work by McCammon et al. [58]. For *A3* and *A4.2*, the search that provided the best exploration was found to be the combination of the genetic algorithm and a local search refinement (GA-LS). The search space was defined using *AutoGrid*, and the same grid was used for all the simulations with the three programs. It was centered in the gorge, between Trp86 and Tyr337, with a size of $82 \times 88 \times 80$ points and a grid spacing of 0.375 Å. The programs *A3* and *A4.2* had the same search parameters: step sizes of 2.0 Å for translation and 50° for rotation. The maximum number of energy evaluations was set to 1×10^7 and the maximum number of generations to 5×10^5 on a single population of 50 individuals. For each compound, 500 geometries were generated and clustered with an RMSD threshold value of 0.5 Å. In the case of *AV* an energy range of 5 kcal/mol was employed, with a maximum number of 10 geometries and an exhaustiveness of 100.

2.3.2. Non-standard residue parameterization

The construction of each of the substrate units to be used in the MD and docking simulations was achieved with the antechamber module, using the GAFF force field [54,59,60] and employing the restricted ESP (RESP) charges obtained from a single point HF/6-31G* [60–62] quantum chemical calculation of the B3LYP/6-31+G* optimized structure within the *Gaussian 03* package [63]. A list of the energies (zero point corrected (ZP)) and *xyz* coordinates of the optimized geometries of the ligands is included in Supplementary material (SM).

2.3.3. MD simulations

The same starting geometry (3LII) [13] was used as in the docking studies. For running the simulations, the ff99 [54] force field was employed and the input files for the simulations were built with the *xleap* package included in *ambertools* [64]. The whole system was neutralized and then solvated with TIP3P [65] water within 8.5 Å around the protein, forming a rectangular box with a total number of 56,000 atoms.

MD simulations were run with the *NAMD* (version 2.8) program [66] at 300 K and applying periodic boundary conditions. Non-bonded interactions were calculated using a 13.0 Å neighboring group list updated every 10 steps of the dynamics. Van der Waals interactions were truncated at 11 Å applying a smooth switching function that started at 8 Å. All electrostatic interactions beyond 11 Å were computed with the particle-mesh Ewald summation [67] and all covalent bonds involving hydrogens were constrained using the SHAKE algorithm [66,68]. The trajectories obtained with *NAMD* were analyzed with *VMD* [69] and the *ambertools* programs [64].

Before starting the MD production stage, three steps were performed. Firstly, two 5000 minimization steps, with the first one keeping the protein heavy atoms restrained at their initial positions and the second one with the whole system free. Secondly, 75 ps of simulation in an NTV ensemble at 300 K were performed, once again with the motion of the protein atoms restrained. After these preparation steps, 20 ns of MD within an NPT ensemble at 300 K were completed. The simulations of the AChEI complexes were run following the same procedure and the starting geometry was obtained from the docking simulations, with the total time of the simulation being 15 ns.

The *python* based scripts implemented in *Amber11* [70] were used to calculate the binding free energies within the molecular mechanic-Poisson–Boltzmann surface area (MM-PBSA) and the molecular mechanic-Generalized Born surface area (MM-GBSA) approximations [71,72]. For these calculations, only the geometries of the last 5 ns of each MD run were taken into account.

3. Results and discussion

3.1. AChE inhibitory activity

The IC_{50} values for **9**, **10** and **11** were determined by the Ellman method [50] following the procedure introduced in Section 2. The results can be observed in Table 1.

3.2. Docking simulations

Before starting the docking simulations, the pK_a of compounds **2**, **9**–**11** were evaluated using a simple approximation [73] whose standard deviation had been previously estimated to be less than 0.5 pK_a units [74]. In all cases, the calculated pK_a values were above 8.3. Therefore, their predominant form, under physiological conditions, was expected to be the protonated one. These were the only states considered for the alkaloids under study. The stabilities of the neutral and protonated stereoisomers of alkaloid **11** with its N-methyl group in either the axial or equatorial position were evaluated by DFT calculations. It was found that the neutral and the protonated forms were more stable with the N-methyl in the axial position, so the geometry of this stereoisomer was employed for the calculations (Scheme 3).

A control search was performed with the complex *Tc*AChE (huprine X) and compared with the experimental one (1E66) [33]. Different algorithms were tested and the parameters within the search were refined, with the best results being obtained with the GA-LS algorithm as described in Section 2. The geometries obtained were close to the experimental one (RMSD difference of 0.55 Å),

Table 1
MM-GBSA calculated binding energies for the AChE complexes, from the MD simulations.

Inhibitor	$E_{binding}$ (kcal/mol)		$\Delta G_{binding}$ (kcal/mol)		IC_{50} (μM)[a]
	AS	PAS	AS	PAS	
9	−27.3 ± 3.3	−27.8 ± 3.2	11.3 ± 3.3	10.2 ± 3.2	Inactive
10	−34.2 ± 2.8	−25.8 ± 2.4	2.6 ± 2.8	12.1 ± 2.4	296.8
11	(a) −38.2 ± 2.5 (b) −41.4 ± 2.7	−25.5 ± 2.0	3.3 ± 2.5 0.5 ± 2.7	16.3 ± 2.0	32.3
2	−47.7 ± 2.8	−30.2 ± 2.3	−8.1 ± 2.8	10.8 ± 2.3	0.082 [83]

[a] Experimental values of IC_{50} are informed in μM. These values were determined according to the Ellman method [50], with some modifications, as described in the experimental section.

thus validating the procedure used. These geometries are presented in Fig. S1 of Supplementary material (SM).

To determine the preferred site for binding of the alkaloids **2**, **9**–**11** in the human AChE, different docking programs were employed. At the first stage, starting from a minimized structure of the enzyme (3LII) [13], the search was carried out within a box including the whole protein. The most stable poses were located in two regions: the AS and the PAS. Accordingly, a smaller grid box was employed in all the docking simulations, taking into account only these two sites in order to obtain refined binding energies and docking poses. To simplify the analysis, the differences in $\Delta G_{binding}$ between the AS and the PAS are represented in Fig. 2. The light bars ($\Delta\Delta G_{binding} < 0$), show a preference for the AS, while the dark ones ($\Delta\Delta G_{binding} > 0$) for the PAS. More details are included in Table S1 of SM.

Although the graphics revealed different tendencies, in most cases the $\Delta\Delta G_{binding}$ were below the estimated error of the *Autodock*'s scoring functions (~2.5 kcal/mol) [52,53]. This has been ascribed to the different scoring functions used, issue that has been previously addressed [9,75,76]. Despite the differences in absolute binding energies, it is important to point out that the top poses obtained for each site were similar for the three docking procedures employed. The results were normalized by rescoring the binding energy of each of the final geometries. In order to carry this out, all the complexes obtained were neutralized with counter ions, solvated and minimized [77] by using the parameters of the ff99 and GAFF force fields. Afterwards, the binding energies were calculated using the MM-PBSA and MM-GBSA approaches [71,72], as proposed by Kunh et al. [78]. After this procedure, the most favored poses corresponded to the proposed inhibitors at the AS site, the exception being compound **9** which had comparable binding energies for the AS and PAS sites, but with a slight discrepancy between MM-GBSA and MM-PBSA.

The geometries of the proposed inhibitors for both sites, obtained after the minimization of the docking geometries, are represented in the SM together with the interactions with the protein residues (Figs. S2–S5) [79,80]. When comparing the poses at the AS, it could be seen that **9** and **10** were almost located in the same place, independently of the position of the substituents. On the other hand, **11** and **2**, despite having similar molecular structures and sizes, adopted different geometries, while **11** had the C and D rings over Trp86 with the carbonyl pointing at the entrance of the gorge, compound **2** had the A and B rings over Trp86, with the third ring being perpendicular and pointing at the entrance of the gorge. This geometry was similar to the one in the X-ray structure of the *Tc*AChE (**2**) complex [35]. An interesting question arose when inspecting the different arrangements adopted by **2** and **11** at the AS. When **11** was put in a conformation similar to that of **2**, a high steric repulsion arose due to the proximity of the CH_2 groups of C9 and C10 to the indole and phenol rings of Trp86 and Tyr337, respectively. This new geometry will be defined as **11b** (geometry of **11** aligned with **2**) and is represented in Fig. S6 of SM. However, when this conformation was forced, and the complex was minimized, a MM-GBSA binding energy of −39.5 kcal/mol (similar to the −38.1 kcal/mol estimated by the same method for the other

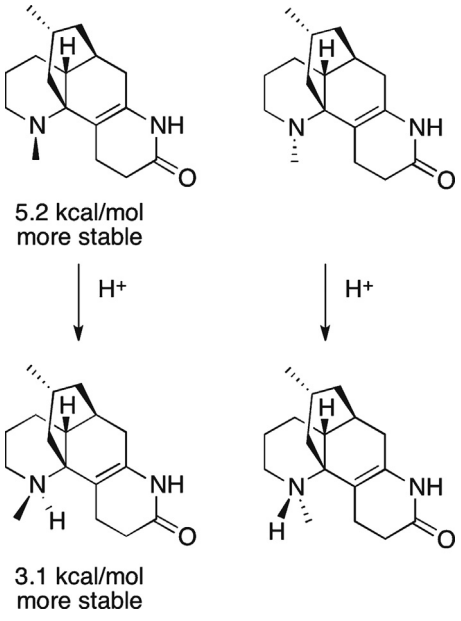

Scheme 3. Different conformers of **11** according to the position of the β-N-methyl group.

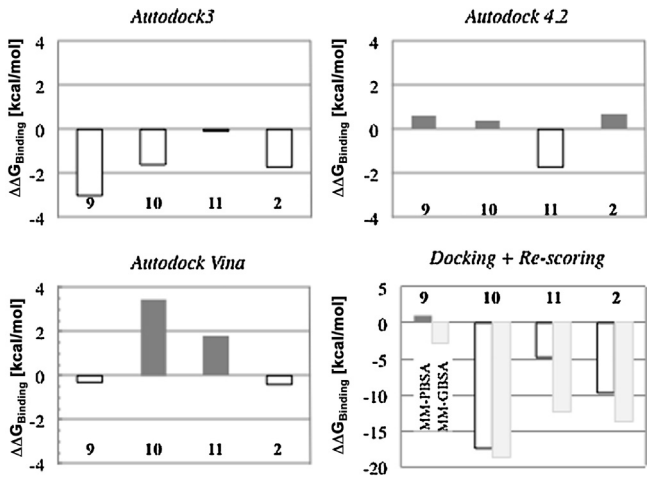

Fig. 2. Preference for the binding at the AS and PAS sites obtained with different procedures. The histograms represent the difference in binding free energies ($\Delta\Delta G_{binding} = \Delta G_{binding\ AS} - \Delta G_{binding\ PAS}$). Light bars show a preference for the AS while dark ones show a predilection for the PAS.

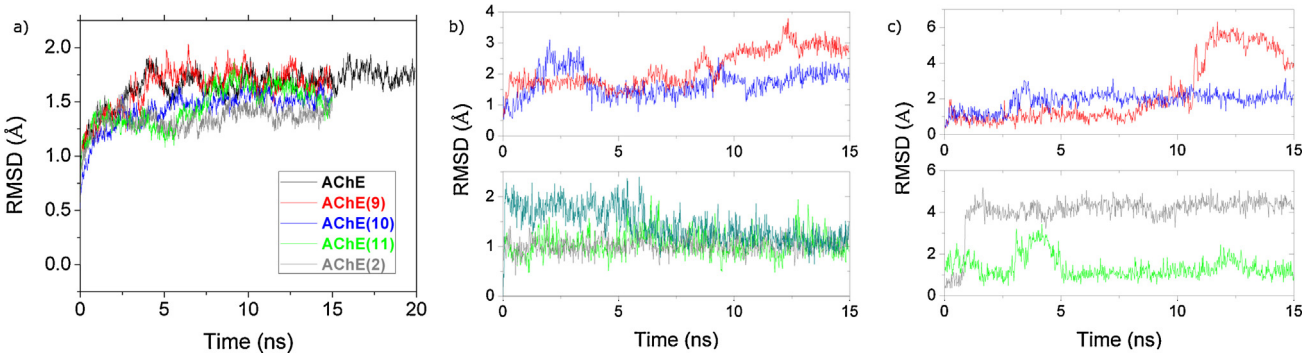

Fig. 3. (a) Evolution of the RMSD of the backbone of the protein for the MD runs of AChE and AChE with compounds **9**–**11** and **2** at the AS. (b) Evolution of the RMSD of the ligands at the AS, without considering the hydrogen atoms. (c) Evolution of the RMSD of the ligands at the PAS, without considering the hydrogen atoms. The same color was employed in all the graphics for representing the properties of each MD run. AChE (■), AChE-**9** (■), AChE-**10** (■), AChE-**11a** (■), AChE-**11b** (■) and AChE-**2** (■).

conformation, see Table S1) was obtained. Based on these results, the new conformation of **11** (**11b**) was also explored by MD simulation and compared with the one obtained by the docking procedure (**11a**). On the other hand, when **2** was forced to adopt the geometry of **11a**, a steric hindrance between the allylic methyl at C10 of **2** and the hydroxyl group of Tyr133 arose, and this new complex afforded a higher binding energy than the one obtained by the original docking conformation (−33.4 vs −40.4 kcal/mol, respectively, after MM-GBSA refinement). These two pairs of geometries are represented in Fig. S7 of SM.

There was no correlation between the binding energies obtained from the docking calculations and the experimental IC_{50} values (see Table 1 of SM). Although refinement and recalculation with MM-PBSA or MM-GBSA improved the results, some discrepancies remained. In an attempt to determine a better correlation with the experimental results, MD studies were carried out for the complexes of the *human* AChE with **2**, **9**–**11** both inside and outside the gorge.

3.3. Molecular dynamic simulations

A simulation of the protein without any ligand was carried out, with the RMSD profiles of the simulations showing, as expected, that the presence of the ligands at the AS or at the PAS did not produce any changes in the global RMSD profiles (Figs. 3 and S8–S10 of SM). As reported in other simulations on the same protein, the RMSD of the backbone and the global one were around 2 and 2.6 Å, respectively [81].

An analysis of the RMSD of the ligands in both sites was performed (Fig. 3b and c), which revealed different profiles inside and outside the gorge related to the topology of the sites. As expected, bigger variations of the RMSD were observed at the PAS, which is a wide place to host the inhibitor.

The binding energies of the MD-complexes were obtained by applying the post-processing methods MM-GBSA and MM-PBSA [71,72]. Recently, it was proposed that even though the performance of these methods may be system dependent, they could still give good results to compare relative binding energies of similar systems [82]. The Poisson–Boltzmann model (PB) is theoretically more rigorous than the Generalized Born model (GB), and hence MM-PBSA is often considered to be naturally superior to MM-GBSA for predicting the free energies of binding. However, in our system, MM-GBSA showed less deviation, and hence for simplicity only the results with this model are presented in Table 1. For informative reasons, the values obtained with MM-PBSA are included in SM, Table S2.

MM-GBSA succeeded in the prediction of **2** and **9** as the best and worst inhibitors, respectively. Moreover, the binding energies in the two explored sites were similar only in the case of **9**. If the binding in the PAS were preferred over AS, then the compound should be inactive or only present a low inhibitory activity, and this indeed may have been the case. For all the other compounds, the binding at the AS was preferred over the PAS. In the case of compound **11**, from the two geometries explored at the AS, the huperzine like geometry (**11b**, Table 1) was more favorable for binding. For **10** and **11a** there were small differences in the binding energies, but the binding of **11**, in its **b** pose, was more favorable even when the entropy was included. It should be noted that after the inclusion of the entropic term, some of the $\Delta G_{binding}$ were positive, probably due to an overestimation of the entropic term. For its evaluation the quasi-harmonic entropy approximation was employed instead of the time consuming normal mode analysis of the harmonic frequencies.

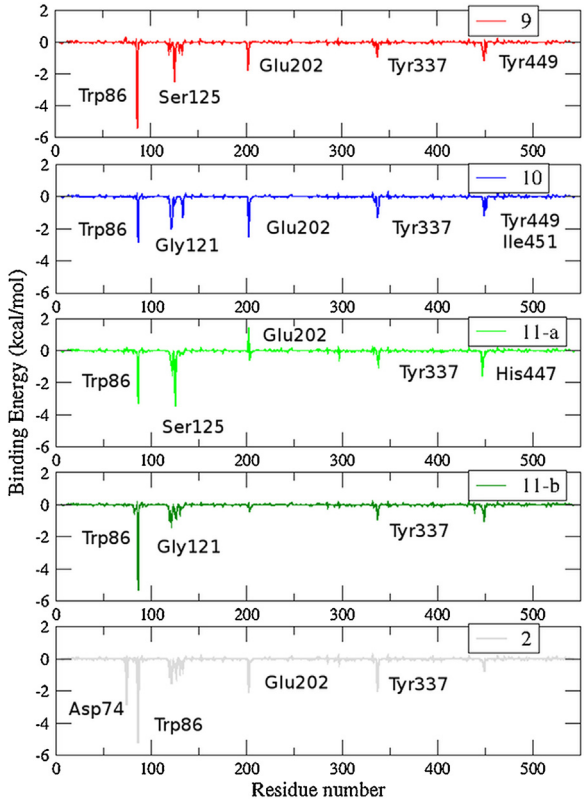

Fig. 4. Per-residue contributions to the binding energy calculated with MM-GBSA from the MD simulations of **9**–**11**, **2** at the AS site. AChE-**9** (■), AChE-**10** (■), AChE-**11a** (■), AChE-**11b** (■) and AChE-**2** (■).

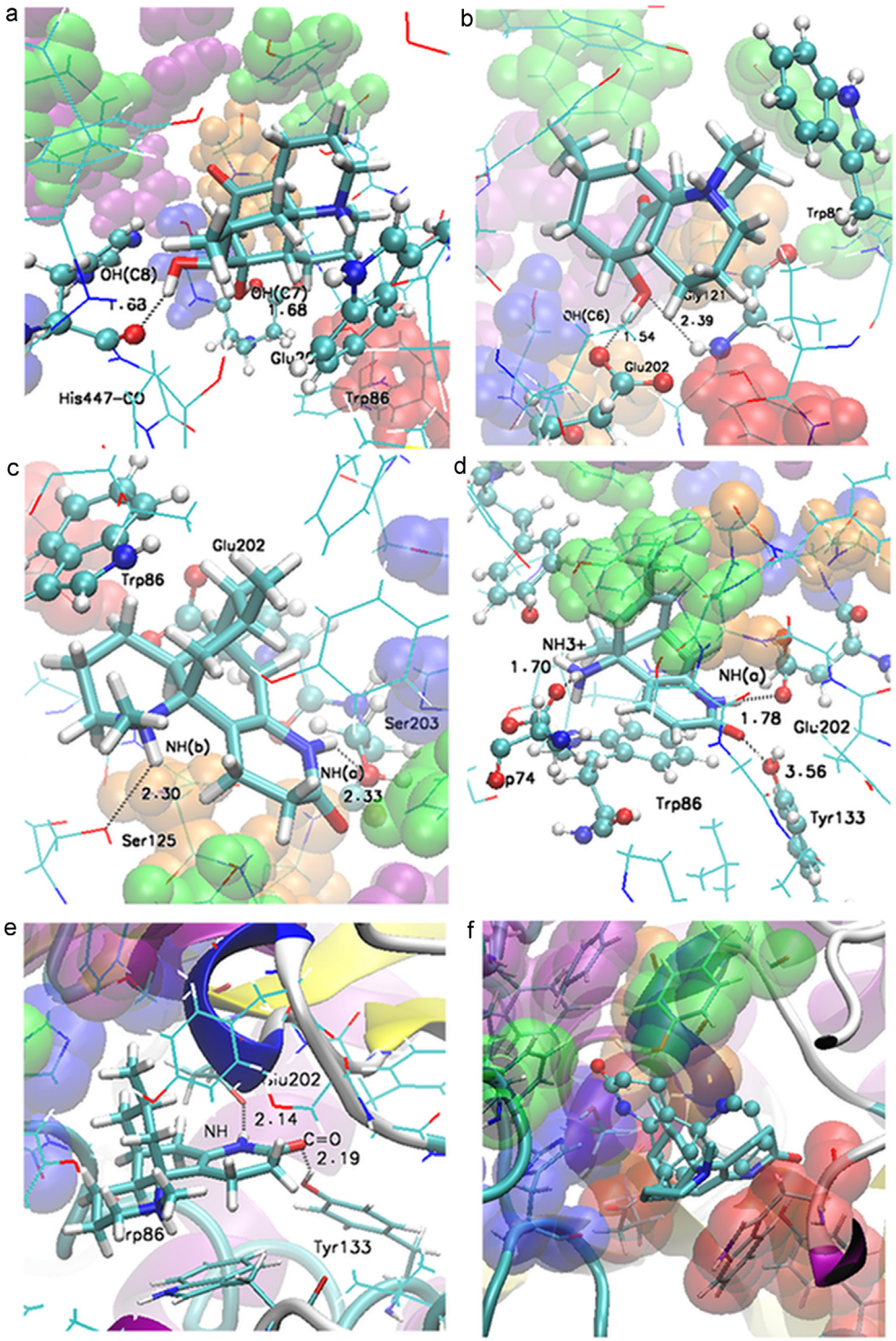

Fig. 5. 3-D plot of the final geometries obtained after 15 ns of MD simulation. For the complexes: (a) AChE-**9**, (b) AChE-**10**, (c) AChE-**11a**, (d) AChE-**2**, (e) AChE-**11b** (similar to **2**). (f) Comparison of the geometries: **11a** (represented with balls and sticks) and **11b** (represented with bold sticks). The hydrogen bonds are represented by black dotted lines.

However, the order of the binding energies was the same as that expected on the basis of the experimental values of IC_{50}.

With the aim of identifying the residues that helped to stabilize the inhibitor of the obtained complexes, a decomposition of the binding energy per residue was performed [84]. A detailed description of this decomposition for the AS is included in Fig. 4, and the main interactions with the protein residues of the AS are shown in Figs. 5 and S11–S15 of SM. This revealed that at the AS site the van der Waals interactions with the indole ring of Trp86 were the most stabilizing ones for almost all the studied compounds (see Fig. 4).

In the case of **9**, the B and D rings and the protonated nitrogen $(R_3NH)^+$ are coplanar with the Trp86 of the anionic subsite (Fig. 5a). The hydroxyl group at C7 formed a hydrogen bond with the carboxylate group of Glu202 during 75% of the MD run, with the other observed stabilizations being due to van der Waals interactions with the aromatic residues Tyr337 and Tyr449 and

those between the oxygen of Ser125 with the CH_2 groups of rings A and B.

As observed for the C7 hydroxyl group of **9**, the OH at C6 of compound **10** also formed a hydrogen bond with the carboxylate of Glu202 throughout the MD run (Fig. 5b). In agreement with the average O—H–O═C distance (1.60 Å), this bond could be considered to be stronger than the one formed by compound **9**, reflected in a bigger stabilizing effect. Besides, the oxygen of this hydroxyl group acted as hydrogen acceptor of the N—H amide group of Gly121, with the interactions with Trp86 and Ser125 being less important. Finally, a similar profile to that of **9** was observed for the van der Waals interactions with Tyr337 and Tyr449.

Several differences may be pointed out by comparing the geometries **11a**–**b** (Fig. 5c, e and f). First, for **11a** the hydrogen bond of β-NH^+ with Ser125 was the most stabilizing contribution, with the α-NH also forming a hydrogen bond with the hydroxyl of Ser203. However, the positive character of β-NH^+ made its interaction markedly stronger. On the other hand, for **11b** β-NH^+ did not form any hydrogen bond, and the van der Waals interactions with Trp86 were the most important. Another important difference was the contribution of Glu202. While for **11a**, no hydrogen bond with Glu202 was formed, thus affording a destabilizing contribution to the binding energy. In the case of **11b**, the hydrogen bond with this residue helped to stabilize the complex even though the interaction did not persist throughout the whole simulation.

Finally, **2** presented van der Waals interactions with Trp86 and Tyr337, in addition to the hydrogen bond between α-NH and the carboxylate of Glu202, and also a new stabilizing component due to the salt bridge between β-NH_3^+ and the carboxylate group of Asp74 (Fig. 5d).

As mentioned above in the simulations of the AChEI complexes with the ligand at the PAS, the inhibitors moved from their initial positions. This fact could be explained due to the topology of the PAS and its exposure to the solvent. The most important interactions at the PAS were those between **9**, **10** and **11** with Trp286 [85]. A per residue decomposition of the interactions of the studied compounds, at the PAS, with the protein is presented in Fig. S16 of SM.

The order of the binding energies for all the studied compounds could be clearly established using the MM-GBSA approach, with **2** being the best inhibitor and **9** the worst. This could also have been related to the order of the IC_{50} values as the right order was obtained with the MM-GBSA approximation. Nevertheless, it is important to remark that this is only one aspect of the binding, and that the kinetic of the entrance as well as that of the exit of the inhibitor from the gorge should also be evaluated as these two processes might play very important roles in the global process of inhibition. Although this is beyond the scope of the present article, it should be born in mind for future studies.

4. Concluding remarks

The Lycopodium alkaloids **10** and **11** have been shown to be inhibitors of the AChE activity, whereas a very similar compound **9** had no inhibitory activity. The binding modes of these inhibitors in AChE were explored with docking calculations, and similar geometries but different binding energies were obtained with the employed programs. Using this approach, a better scoring was obtained to improve the quality of the estimation of the binding energy by incorporating an all atom force field and the MM-GBSA (MM-PBSA) methods for its calculation. This refinement permitted a better discrimination between the active and inactive compounds, with the binding preferences for the AS and the PAS sites.

Molecular dynamics simulations were carried out for the AChE complexes with the alkaloids **9**–**11** and **2**, and the binding modes at both sites of the protein were studied. MM-GBSA succeeded in ordering the alkaloids according to their inhibitory activities or binding energies. The lack of activity in **9** may be ascribed to the similar binding energies for the AS and the PAS, and the compounds with higher activities presented higher affinities for the AS than the PAS.

Acknowledgments

This work was supported in part by the Consejo Nacional de Investigaciones Científicas y Tecnológicas (CONICET), the Agencia Nacional de Promoción Científica y Tecnológica (FONCYT, Argentina), the Agencia Córdoba Ciencia and the Secretaría de Ciencia y Técnica (SECYT) of the Universidad Nacional de Córdoba. INFIQC and IMBIV are jointly sponsored by CONICET and the Universidad Nacional de Córdoba. All calculations were performed with time allocation on the *Cristina* supercomputer, built through an ANPCYT special funding (grant PME-2006-01581). J.L.B. gratefully acknowledges the receipt of a PhD fellowship from CONICET. We thank Dr. Paul David Hobson, native speaker, for revision of the manuscript.

Appendix A. Supplementary data

Supplementary data associated with this article can be found, in the online version, at http://dx.doi.org/10.1016/j.jmgm.2013.05.009.

References

[1] C. Mount, C. Downton, Alzheimer's disease: progress or profit? Nature Medicine 12 (2006) 780–784.
[2] C. Haas, Strategies, development, and pitfalls of therapeutic options for Alzheimer's disease, Journal of Alzheimer's Disease 28 (2012) 241–281.
[3] P.J. Whitehouse, D.L. Price, R.G. Struble, A.W. Clark, J.T. Coyle, M.R. Delon, Alzheimer's disease and senile dementia: loss of neurons in the basal forebrain, Science 215 (1982) 1237–1239.
[4] N.C. Inestrosa, A. Alvarez, C.A. Pérez, R.D. Moreno, M. Vicente, C. Linker, et al., Acetylcholinesterase accelerates assembly of amyloid-β-peptides into Alzheimer's fibrils: possible role of the peripheral site of the enzyme, Neuron 16 (1996) 881–891.
[5] A. Alvarez, F. Bronfman, C.A. Pérez, M. Vicente, J. Garrido, N.C. Inestrosa, Acetylcholinesterase, a senile plaque component, affects the fibrillogenesis of amyloid-β-peptides, Neuroscience Letters 201 (1995) 49–52.
[6] D. Muñoz-Torrero, Acetylcholinesterase inhibitors as disease-modifying therapies for Alzheimers disease, Current Medicinal Chemistry 15 (2008) 2433–2455.
[7] X.-L. Zhu, N.-X. Yu, G.-F. Hao, W.-C. Yang, G.-F. Yang, Structural basis of femtomolar inhibitors for acetylcholinesterase subtype selectivity: insights from computational simulations, Journal of Molecular Graphics and Modelling 41 (2013) 55–60.
[8] A.J. Bermúdez-Lugo, C.M. Rosales-Hernandez, O. Deeb, J. Trujillo-Ferrara, J. Correa-Basurto, In silico methods to assist drug developers in acetylcholinesterase inhibitor design, Current Medicinal Chemistry 18 (2011) 1122–1136.
[9] H. Zaheer-ul, S.A. Halim, R. Uddin, J.D. Madura, Benchmarking docking and scoring protocol for the identification of potential acetylcholinesterase inhibitors, Journal of Molecular Graphics and Modelling 28 (2010) 870–882.
[10] M.T.H. Khan, Molecular interactions of cholinesterases inhibitors using in silico methods: current status and future prospects, New Biotechnology 25 (2009) 331–346.
[11] J. Muñoz-Muriedas, J.M. López, M. Orozco, F.J. Luque, Molecular Modelling approaches to the design of acetylcholinesterase inhibitors: new challenges for the treatment of Alzheimer's disease, Current Pharmaceutical Design 10 (2004) 3131–3140.
[12] J.L. Sussman, M. Harel, F. Frolow, C. Oefner, A. Goldman, L. Toker, et al., Atomic structure of acetylcholinesterase from *Torpedo californica*: a prototypic acetylcholine-binding protein, Science 253 (1991) 872–879.
[13] H. Dvir, I. Silman, M. Harel, T.L. Rosenberry, J.L. Sussman, Acetylcholinesterase: from 3D structure to function, Chemico-Biological Interactions 187 (2010) 10–22.
[14] I. Silman, J.L. Sussman, Acetylcholinesterase: how is structure related to function? Chemico-Biological Interactions 175 (2008) 3–10.
[15] The numeration of the residues corresponds to the human AChE.

[16] G.V. De Ferrari, M.A. Canales, I. Shin, L.M. Weiner, I. Silman, N.C. Inestrosa, A Structural motif of acetylcholinesterase that promotes amyloid β-peptide fibril formation, Biochemistry 40 (2001) 10447–10457.
[17] E. Giacobini, Cholinesterase inhibitors stabilize Alzheimer disease, Neurochemical Research 25 (2000) 1185–1190.
[18] M. Bartolini, C. Bertucci, V. Cavrini, V. Andrisano, β-Amyloid aggregation induced by human acetylcholinesterase: inhibition studies, Biochemical Pharmacology 65 (2003) 407–416.
[19] P. Williams, A. Sorribas, M.J.R. Howes, Natural products as a source of Alzheimer's drug leads, Natural Product Reports 28 (2011) 48–77.
[20] M.R. Loizzo, R. Tundis, F. Conforti, F. Menichini, M. Bonesi, F. Nadjafi, et al., *Salvia leriifolia Benth* (*Lamiaceae*) extract demonstrates in vitro antioxidant properties and cholinesterase inhibitory activity, Nutrition Research 30 (2010) 823–830.
[21] M.G. Ortega, A.M. Agnese, J.L. Cabrera, Anticholinesterase activity in an alkaloid extract of *Huperzia saururus*, Phytomedicine 11 (2004) 539–543.
[22] L.J. Thal, P.A. Fuld, D.M. Masur, N.S. Sharpless, Oral physostigmine and lecithin improve memory in Alzheimer disease, Annals of Neurology 13 (1983) 491–496.
[23] J.-S. Liu, Y.-L. Zhu, C.-M. Yu, Y.-Z. Zhou, Y.-Y. Han, F.-W. Wu, et al., The structures of huperzine A and B, two new alkaloids exhibiting marked anticholinesterase activity, Canadian Journal of Chemistry 64 (1986) 837–839.
[24] G.T. Ha, R.K. Wong, Y. Zhang, Huperzine A as potential treatment of Alzheimer's disease: an assessment on chemistry, pharmacology, and clinical studies, Chemistry and Biodiversity 8 (2011) 1189–1204.
[25] G.K. Wilcock, S. Lilienfeld, E. Gaens, Efficacy and safety of galantamine in patients with mild to moderate Alzheimer's disease: multicentre randomised controlled trial, British Medical Journal 321 (2000) 1445.
[26] H.-G. Boit, Über die Alkaloide der Zwiebeln von Galanthus nivalis (III. Mitteil. über Amaryllidaceen-Alkaloide), Chemische Berichte 87 (1954) 724–725.
[27] A. Albert, W. Gledhill, Improved syntheses of aminoacridines. Part IV. Substituted 5-aminoacridines, Journal of the Society of Chemical Industry 64 (1945) 169–172.
[28] H. Sugimoto, H. Ogura, Y. Arai, Y. Limura, Y. Yamanishi, Research and development of donepezil hydrochloride, a new type of acetylcholinesterase inhibitor, Japanese Journal of Pharmacology 89 (2002) 7–20.
[29] S.L. Rogers, L.T. Friedhoff, The efficacy and safety of donepezil in patients with Alzheimer's disease: results of a US Multicentre, Randomized, Double-Blind, Placebo-Controlled Trial. The Donepezil Study Group, Dementia 7 (1996) 293–303.
[30] R. Moretti, P. Torre, R.M. Antonello, G. Cazzato, Rivastigmine in subcortical vascular dementia: a comparison trial on efficacy and tolerability for 12 months follow-up, European Journal of Neurology 8 (2001) 361–362.
[31] P. Camps, D. Muñoz-Torrero, Tacrine–Huperzine A hybrids (Huprines) A new class of highly potent and selective acetylcholinesterase inhibitors of interest for the treatment of Alzheimer disease, Mini-Reviews in Medicinal Chemistry 1 (2001) 163–174.
[32] P. Camps, R. El Achab, D.M. Görbig, J. Morral, D. Muñoz-Torrero, A. Badia, et al., Synthesis, in vitro pharmacology, and molecular modeling of very potent tacrine–huperzine A hybrids as acetylcholinesterase inhibitors of potential interest for the treatment of Alzheimer's disease, Journal of Medicinal Chemistry 42 (1999) 3227–3242.
[33] H. Dvir, D.M. Wong, M. Harel, X. Barril, M. Orozco, F.J. Luque, et al., 3D structure of *Torpedo californica* acetylcholinesterase complexed with huprine X at 2.1 Å resolution: kinetic and molecular dynamic correlates, Biochemistry 41 (2002) 2970–2981.
[34] P. Camps, B. Cusack, W.D. Mallender, R. El Achab, J. Morral, D. Muñoz-Torrero, et al., Huprine X is a novel high-affinity inhibitor of acetylcholinesterase that is of interest for treatment of Alzheimer's disease, Molecular Pharmacology 57 (2000) 409–417.
[35] H. Dvir, H.L. Jiang, D.M. Wong, M. Harel, M. Chetrit, X.C. He, et al., X-ray structures of *Torpedo californica* acetylcholinesterase complexed with (+)-huperzine A and (−)-huperzine B: structural evidence for an active site rearrangement, Biochemistry 41 (2002) 10810–10818.
[36] P. Bar-On, C.B. Millard, M. Harel, H. Dvir, A. Enz, J.L. Sussman, et al., Kinetic and structural studies on the interaction of cholinesterases with the anti-Alzheimer drug rivastigmine, Biochemistry 41 (2002) 3555–3564.
[37] C. Bartolucci, E. Perola, C. Pilger, G. Fels, D. Lamba, Three-dimensional structure of a complex of galanthamine (Nivalin®) with acetylcholinesterase from *Torpedo californica*: implications for the design of new anti-Alzheimer drugs, Proteins 42 (2001) 182–191.
[38] M.L. Raves, M. Harel, Y.-P. Pang, I. Silman, A.P. Kozikowski, J.L. Sussman, Structure of acetylcholinesterase complexed with the nootropic alkaloid, (−)-huperzina A, Nature Structural Biology 4 (1997) 57–63.
[39] J.-M. López-Castillo, A. Filali-Mouhim, É. Nguyen Van Binh-Otten, J.-P. Jay-Gerin, Electron transfer in proteins: structural and energetic control of the electronic coupling, Journal of American Chemical Society 119 (1997) 1978–1980.
[40] M. Harel, I. Schalk, L. Ehret-Sabatier, F. Bouet, M. Goeldner, C. Hirth, et al., Acetylcholinesterase, Alzheimer's disease, crystal structure, drug–protein complex, Proceeding of the National Academy of Sciences of the United States of America 90 (1993) 9031–9035.
[41] X. Ma, D.R. Gang, The Lycopodium alkaloids, Natural Product Reports 21 (2004) 752–772.
[42] J.L. Amorín, Cola de Quirquincho Urostachis saururus (Lam) Herter (Lycopodiaceas) Una peligrosa planta usada en la medicina popular Argentina, Farmacobotánica 16 (1974) 3–6.
[43] R. Martinez Crovetto, Las Plantas utilizadas en medicina popular, Miscelanea 69 (1981) 15.
[44] M.G. Ortega, A.M. Agnese, J.L. Cabrera, Sauroine a novel Lycopodium alkaloid from *Huperzia saururus*, Tetrahedron Letters 45 (2004) 7003–7005.
[45] M.G. Vallejo, M.G. Ortega, J.L. Cabrera, V.P. Carlini, S. Rubiales de Barioglio, R.S. Almirón, et al., Sauroine, an alkaloid from *Huperzia saururus* with activity in Wistar rats in electrophysiological and behavioral assays related to memory retention, Journal of Natural Products 72 (2009) 156–158.
[46] M.G. Vallejo, M.G. Ortega, J.L. Cabrera, V. Carlini, S. Barioglio, A.M. Agnese, *Huperzia saururus* increases memory retention in rats, Journal of Ethnopharmacology 111 (2007) 685–687.
[47] E.S. Halldorsdottir, J.W. Jaroszewski, E.S. Olafsdottir, Acetylcholinesterase inhibitory activity of lycopodane-type alkaloids from the Icelandic *Lycopodium annotinum* ssp. alpestre, Phytochemistry 71 (2010) 149–157.
[48] W.A. Ayer, L.S. Trifonov, Chapter 3: Lycopodium alkaloids, in: A.C. Geoffrey, B. Arnold (Eds.), The Alkaloids: Chemistry and Pharmacology, vol. 45, Academic Press, 1994, pp. 233–266.
[49] W.A. Ayer, T.E. Habgood, V. Deulofeu, H.R. Juliani, Lycopodium alkaloids: sauroxine, Tetrahedron 21 (1965) 2169–2172.
[50] G.L. Ellman, K.D. Courtney, V. Andres Jr., R.M. Featherstone, A new and rapid colorimetric determination of acetylcholinesterase activity, Biochemical Pharmacology 7 (1961) 88–95.
[51] G.M. Morris, D.S. Goodsell, R.S. Halliday, R. Huey, W.E. Hart, R.K. Belew, et al., Automated docking using a Lamarckian genetic algorithm and an empirical binding free energy function, Journal of Computational Chemistry 19 (1998) 1639–1662.
[52] G.M. Morris, R. Huey, W. Lindstrom, M.F. Sanner, R.K. Belew, D.S. Goodsell, et al., AutoDock4 and AutoDockTools4: automated docking with selective receptor flexibility, Journal of Computational Chemistry 30 (2009) 2785–2791.
[53] O. Trott, A.J. Olson, AutoDock Vina: improving the speed and accuracy of docking with a new scoring function, efficient optimization, and multithreading, Journal of Computational Chemistry 31 (2010) 455–461.
[54] J. Wang, P. Cieplak, P.A. Kollman, How well does a restrained electrostatic potential (RESP) model perform in calculating conformational energies of organic and biological molecules? Journal of Computational Chemistry 21 (2000) 1049–1074.
[55] M.P. Jacobson, D.L. Pincus, C.S. Rapp, T.J.F. Day, B. Honig, D.E. Shaw, et al., A hierarchical approach to all-atom protein loop prediction, Proteins 55 (2004) 351–367.
[56] J. Myers, G. Grothaus, S. Narayanan, A. Onufriev, A simple clustering algorithm can be accurate enough for use in calculations of pKs in macromolecules, Proteins 63 (2006) 928–938.
[57] J.C. Gordon, J.B. Myers, T. Folta, V. Shoja, L.S. Heath, A. Onufriev, H++: a server for estimating pK_as and adding missing hydrogens to macromolecules, Nucleic Acids Research 33 (2005) W368–W371.
[58] S.T. Wlodek, T.W. Clark, L.R. Scott, J.A. Mccammon, Molecular dynamics of acetylcholinesterase dimer complexed with tacrine, Science 7863 (1997) 9513–9522.
[59] J. Wang, R.M. Wolf, J.W. Caldwell, P.A. Kollman, D.A. Case, Development and testing of a general amber force field, Journal of Computational Chemistry 25 (2004) 1157–1174.
[60] W.D. Cornell, P. Cieplak, C.I. Bayly, I.R. Gould, K.M. Merz, D.M. Ferguson, et al., A second generation force field for the simulation of proteins, nucleic acids, and organic molecules, Journal of American Chemical Society 117 (1995) 5179–5197.
[61] C.I. Bayly, P. Cieplak, W. Cornell, P.A. Kollman, A well-behaved electrostatic potential based method using charge restraints for deriving atomic charges: the RESP model, Journal of Physical Chemistry 97 (1993) 10269–10280.
[62] W.D. Cornell, P. Cieplak, C.I. Bayly, P.A. Kollmann, Application of RESP charges to calculate conformational energies, hydrogen bond energies, and free energies of solvation, Journal of Physical Chemistry 115 (1993) 9620–9631.
[63] M.J. Frisch, G.W. Trucks, H.B. Schlegel, G.E. Scuseria, M.A. Robb, J.R. Cheeseman, et al., GAUSSIAN 03 (Revision B.04), Gaussian, Inc., Wallingford, CT, 2003 http://www.gaussian.com
[64] D.A. Case, T.A. Darden, T.E. Cheatham III, C.L. Simmerling, J. Wang, R.E. Duke, R. Luo, R.C. Walker, W. Zhang, K.M. Merz, B. Roberts, S. Hayik, A. Roitberg, G. Seabra, J. Swails, A.W. Goetz, I. Kolossváry, K.F. Wong, F. Paesani, J. Vanicek, R.M. Wolf, J. Liu, X. Wu, S.R. Brozell, T. Steinbrecher, H. Gohlke, Q. Cai, X. Ye, J. Wang, M.-J. Hsieh, G. Cui, D.R. Roe, D.H. Mathews, M.G. Seetin, R. Salomon-Ferrer, C. Sagui, V. Babin, T. Luchko, S. Gusarov, A. Kovalenko, P.A. Kollman, AMBER 12, University of California, San Francisco, 2012.
[65] W.L. Jorgensen, J. Chandrasekhar, J.D. Madura, R.W. Impey, M.L. Klein, Comparison of simple potential functions for simulating liquid water, Journal of Chemical Physics 79 (1983) 926.
[66] J.C. Phillips, R. Braun, W. Wang, J. Gumbart, E. Tajkhorshid, E. Villa, et al., Scalable molecular dynamics with NAMD, Journal of Computational Chemistry 26 (2005) 1781–1802.
[67] A.A. Golosov, M. Karplus, Probing polar solvation dynamics in proteins: a molecular dynamics simulation analysis, Journal of Physical Chemistry B 111 (2007) 1482–1490.
[68] J.-P. Ryckaert, G. Ciccotti, H.J.C. Berendsen, Numerical integration of the Cartesian equations of motion of a system with constraints: molecular dynamics of n-alkanes, Journal of Computational Chemistry 23 (1977) 327–341.
[69] W. Humphrey, A. Dalke, K. Schulten, VMD: visual molecular dynamics, Journal of Molecular Graphics 14 (1996) 33–38.

[70] D.A. Case, T.A. Darden, I.T.E. Cheatham, C.L. Simmerling, J. Wang, R.E. Duke, et al., AMBER 11, University of California, San Francisco, 2010.
[71] P.A. Kollman, I. Massova, C. Reyes, B. Kuhn, S. Huo, L. Chong, et al., Calculating structures and free energies of complex molecules: combining molecular mechanics and continuum models, Accounts of Chemical Research 33 (2000) 889–897.
[72] J. Srinivasan, T.E. Cheatham, P. Cieplak, P.A. Kollman, D.A. Case, Continuum solvent studies of the stability of DNA, RNA, and phosphoramidate-DNA helices, Journal of American Chemical Society 120 (1998) 9401–9409.
[73] S.H. Hilal, S.W. Karickhoff, L.A. Carreira, A rigorous test for SPARC's Chemical reactivity models: estimation of more than 4300 ionization pK_as, Quantitative Structure–Activity Relationships 14 (1995) 348–355.
[74] M. Remko, M. Swart, F.M. Bickelhaupt, Theoretical study of structure, pK_a, lipophilicity, solubility, absorption, and polar surface area of some centrally acting antihypertensives, Bioorganic and Medicinal Chemistry 14 (2006) 1715–1728.
[75] P.A. Holt, J.B. Chaires, J.O. Trent, Molecular docking of intercalators and groove-binders to nucleic acids using Autodock and Surflex, Journal of Chemical Information and Modeling 48 (2008) 1602–1615.
[76] E. Yuriev, M. Agostino, P.A. Ramsland, Challenges and advances in computational docking: 2009 in review, Journal of Molecular Recognition 24 (2011) 149–164.
[77] The followed procedure is the same one used in the preparation of the geometries for the MD simulations.
[78] B. Kuhn, P. Gerber, T. Schulz-Gasch, M. Stahl, Validation and use of the MM-PBSA approach for drug discovery, Journal of Medicinal Chemistry 48 (2005) 4040–4048.
[79] Two different representations of these geometries are included, one of these in 2-D, plotted with the ligplot software and showing the interactions with the protein residues.
[80] R.A. Laskowski, M.B. Swindells, LigPlot+: multiple ligand–protein interaction diagrams for drug discovery, Journal of Chemical Information and Modeling 51 (2011) 2778–2786.
[81] Y. Xu, J.P. Colletier, M. Weik, H. Jiang, J. Moult, I. Silman, et al., Flexibility of aromatic residues in the active-site gorge of acetylcholinesterase: X-ray versus molecular dynamics, Biophysical Journal 95 (2008) 2500–2511.
[82] T. Hou, J. Wang, Y. Li, W. Wang, Assessing the performance of the MM/PBSA and MM/GBSA methods. 1. The accuracy of binding free energy calculations based on molecular dynamics simulations, Journal of Chemical Information and Modeling 51 (2011) 69–82.
[83] D.L. Bai, X.C. Tang, X.C. He, Huperzine A, a potential therapeutic agent for treatment of Alzheimer's disease, Current Medicinal Chemistry 7 (2000) 355–374.
[84] H. Gohlke, C. Kiel, D.A. Case, Insights into protein–protein binding by binding free energy calculation and free energy decomposition for the Ras–Raf and Ras–RalGDS complexes, Journal of Molecular Biology 330 (2003) 891–913.
[85] Compound **2** moved toward the entrance of the gorge instead of being placed over Trp86, and that is why this interaction is not the most important one. See Fig. S17 of SM.